Journal of Solid State Chemistry 266 (2018) 217–225

Contents lists available at ScienceDirect

Journal of Solid State Chemistry

journal homepage: www.elsevier.com/locate/jssc

# Computational simulations of ZnO@GaN and GaN@ZnO core@shell nanotubes

N.L. Marana[a,*], S. Casassa[b], E. Longo[c], J.R. Sambrano[a]

[a] Modeling and Molecular Simulations Group, CDMF, São Paulo State University, UNESP, Bauru, SP, Brazil
[b] Theoretical Group of Chemistry, Chemistry Department, Torino University, Torino, Italy
[c] Chemistry Institute – CDMF, Federal University of São Carlos, São Carlos, SP, Brazil

ARTICLE INFO

*Keywords:*
Core@shell
Nanotube
Interface
Double-walled

ABSTRACT

The structural, electronic, and mechanical properties of armchair and zigzag chiralities double-walled and core@shell ZnO@GaN and GaN@ZnO nanotubes were investigated by periodic DFT/B3LYP calculations with an all-electron basis set. For both chiralities, GaN@ZnO presents minor strain and deposition energies, which predict that this nanotube can be easier formed and the GaN is the most favorable substrate (the core) than ZnO. On the other hand, the zigzag GaN@ZnO did not exhibit the major piezoelectric response, which is three times smaller than the ZnO@GaN nanotube, showing that the compression of the core@shell nanotube length is not favorable to this property. However, the piezoelectricity can be improved when the zigzag GaN@ZnO is under elongation. The elastic constants showed that the core@shell nanotubes are more rigid than the homogenous nanotubes and present higher piezoelectric constants. In addition, the projected DOS shows that GaN@ZnO has a type-II interface and ZnO@GaN has a type-I interface. Based on the results obtained from our theoretical models, the nanotubes have great potential for the experimental development of new electronic devices.

## 1. Introduction

Zinc oxide (ZnO) is a semiconductor material that presents a wide and diverse range of applications due to its intrinsic properties. ZnO is a *n*-type semiconductor [1] owing to the stoichiometric deviation generated by oxygen vacancies and/or interstitial zinc atoms. The high-quality of ZnO *p*-type is very difficult to be obtain due to the self-compensation issue. In this sense, ZnO *pn*-type semiconductor is only possible through the junctions with a *p*-type material. However, *pn*-type materials have promising applications as rectifier diodes, bipolar transistors, solar cells, light-emitting diodes, and photodetectors, for which they have several advantages such as low dark current, fast response time, and high responsivity.

*p*-Type gallium nitride (GaN) is an ideal candidate to create a *pn*-type junction with ZnO. Both ZnO and GaN exhibit similar semiconducting behavior with band gaps of 3.2 eV and 3.4 eV, respectively, a slight lattice mismatch (~ 1.86%), and spontaneous polarization [2] in addition to similar electrical and piezoelectric properties, which are features that make their application in different electronic and optoelectronic devices possible [3–6].

The fabrication of the *pn*-junction of ZnO and GaN has been reported by many experimental research groups, who obtained ZnO@GaN core@shell structures through low-pressure metal-organic vapor-phase epitaxy (MOVPE) [7], low-temperature approaches [8], vapor-liquid-solid processes [9], and most commonly, by metal-organic chemical vapor deposition (MOCVD) [10,11]. Moreover, many theoretical research groups have analyzed the main properties of these structures using different methodologies [12–14].

There are, however, only few theoretical studies on ZnO@GaN core@shell structures. The ZnO@GaN (0001) surface shows that the junction presents spontaneous polarization and piezoelectric properties. The difference in polarization between ZnO and GaN induces a surface charge, resulting in the accumulation of band electrons at the N-polar interface [15]. In addition, a band alignment study of the ZnO@GaN surfaces revealed a type-II behavior, which comprises the separation of nitrogen and gallium in the valence band (VB) and of zinc and oxygen in the conduction band (CB) [16].

ZnO@GaN superlattice nanowires were also theoretically investigated to understand their electronic and magnetic properties, which arise because of the defects at the interface [17]. When the Ga-O interface is doped with *p*-type elements (Zn or N), ferromagnetism is induced, and the band gap is reduced owing to the type-II alignment.

* Corresponding author.
*E-mail address:* namarana@fc.unesp.br (N.L. Marana).

https://doi.org/10.1016/j.jssc.2018.07.023
Received 24 April 2018; Received in revised form 16 June 2018; Accepted 20 July 2018
Available online 24 July 2018

In addition, the stability and band gap of the nanowire depends on the GaN units, and as the number of GaN units increases, the stability decreases [18].

Lim and coworkers have theoretically analyzed the Zn and O co-doping of GaN nanotubes at different concentrations and in different directions [19]. Their study showed that the best doping concentration is about 31 atomic percent (at%) for single-walled armchair nanotubes and 21 at% for zigzag nanotubes, leading to a widely tunable band gap, enhanced mobility, and better band edge alignments. Moreover, Chai and co-authors showed that armchair and zigzag GaN@ZnO nanotubes are light-emitters in the UV region and are potential photocatalysts for water splitting [20].

ZnO nanotubes grown on a GaN substrate were also investigated [21,22]. Lee et al. synthetized ZnO@GaN nanotubes by heteroepitaxial growth on a Si/GaN substrate for application as micro-LEDs that were obtained by the overlay of the prepared ZnO@GaN nanotubes with a *p*-GaN layer [23]. The micro-LEDs obtained were high-quality coaxial nanotube heterostructures without defects that emitted green light, thereby forming visible light microemitters with a dominant peak at 2.35 eV in the electromagnetic spectrum at room temperature.

Although there are numerous studies on ZnO@GaN or GaN@ZnO core@shell systems, there are only a few reports on the corresponding nanotubes and, to the best of our knowledge, there are no reports on the *pn*-junction of double-walled (DW) ZnO@GaN or GaN@ZnO nanotubes simulated with a model where (i) GaN and ZnO have the same concentration, (ii) Zn-N and Ga-O chemical bonds are formed between the two moieties, and (iii) the coating of a nanotube is simulated by replacing the outer layer with the second material.

Therefore, the aim of this work was to analyze the feasibility and stability of DW ZnO@GaN and GaN@ZnO nanotubes by means of periodic Density Functional Theory (DFT) calculations and to evaluate their unique structural, electronic, elastic, and piezoelectric properties. The effect of the two different inner/outer arrangements, referred herein as the core@shell models, will be emphasized and discussed. In particular, changes in the electron density, $\rho(r)$, were monitored through the analysis of topological properties according to the Quantum Theory of Atoms in Molecules and Crystals, QTAIMAC [24,25]. Ultimately, this work intends to show the way for the synthesis of nanotubes with the best performance for application in electronic devices.

## 2. Computational methods

DFT simulations were conducted using the CRYSTAL14 program [26] with the B3LYP hybrid functional [27] and the all-electron 86-411d31G [28], 8-411d1 [29], 86-4111d41G [30], and 6–21G* [31] basis sets to describe zinc, oxygen, gallium, and nitrogen atoms, respectively.

DFT has emerged as a computational approach of comparable accuracy to the traditional correlated quantum mechanical methods. In this formalism, the exchange and correlation terms are described by a functional of the density and the computational cost is comparable to a Hartree–Fock calculation. Since the precise form of the exchange-correlation functional is unknown, several exchange-correlation functionals have been proposed to approximate the exact functional. In particular, the B3LYP choice was made taking into account a previous work (see Ref. [32]), in which a different functional was tested in order to obtain the best results about the structural and electronic parameters. In this sense, the functional that presented the best relation accuracy/computational cost was the B3LYP functional. Also, this methodology has been used in different investigations and has provided the best approximations to the experimental band gap energy, lattice and internal parameters of zinc oxide and gallium nitride [32–36].

The integration process was performed using the option XXLGRID (extra-extra-large grid), available on CRYSTAL14, containing 99 radial and 1454 angular points. The accuracy of the truncation criterion for the bio-electronic integrals (Coulomb and HF exchange series) was controlled by a set of five thresholds ($10^{-8}$, $10^{-8}$, $10^{-8}$, $10^{-8}$, and $10^{-16}$). These parameters respectively represent the overlap and penetration of the Coulomb integrals, the overlap of the HF exchange integrals, and the last two are the pseudo-overlap in the HF exchange series. In the self-consistent field (SCF) procedure, the shrinking factor for both the diagonalization of the Fock matrix and the calculation of the energy was set to 6, corresponding to 4 independent k-points in the irreducible part of the Brillouin zone. The total and projected density of state (DOS) and the band structure were plotted employing the same k-point sampling as the SCF procedure.

The elastic and piezoelectric constants were also calculated. In the CRYSTAL code, the polarization can be computed either via localized Wannier functions or via the Berry phase (BP) approach [26].

The elastic tensor is usually defined as:

$$\boldsymbol{C}_{vu} = \frac{\mathbf{1}}{\boldsymbol{V}} \frac{\partial^2 \boldsymbol{E}}{\partial \boldsymbol{n}_v \boldsymbol{n}_u}\bigg|_{\mathbf{0}} \tag{1}$$

where $n$ is the rank-2 symmetric tensor of pure strain and Voigt's notation is used according to which $v$, $u = 1, 2,..., 6$, and $V$ the volume of the cell structure. Second derivatives in Eq. (1) are computed as first numerical derivatives of analytical energy gradients in the present implementation.

However, for the 1D systems (as nanotube), the volume can be calculated as:

$$V = 2\pi R l d \tag{2}$$

were $R$ being the nanotube radium, $l$ nanotube length, and $d$ the sum of the bond length and van der Waals radius of the atoms [37]. It should be noted that all the elements involving non-periodic directions ($y$ and $z$ for 1D systems) are null by definition, therefore, the only calculated elastic constant is $c_{11}$.

In the linear regime, the direct $e$ piezoelectric tensor describes the polarization $P$ induced by strain ($n$), which is induced by an external electric field $E$ at constant electric field, i. e: $P = ne$. Then, the Cartesian components of the polarization can be expressed as follows in terms of the strain tensor components:

$$P_i = \sum_v e_{iv} n_v, \text{ so that: } e_{iv} = \left(\frac{\partial P_i}{\partial n_v}\right)_E \tag{3}$$

in the above expression, $i = 1,..., 3$; $n$ is according to pure strain tensor, the derivative is taken at constant electric field and Voigt's notation is used. In the present work, as mentioned above, the polarization was calculated via BP approach, in terms of numerical first derivatives of the BP $\varphi_l$ with respect to the strain:

$$e_{iv} = \frac{|e|}{2\pi V} \sum_l a_{li} \frac{\partial \varphi_l}{\partial n_v} \tag{4}$$

where $a_{li}$ is the $i$-th Cartesian component of the $l$-th direct lattice basis vector $a_l$. Such as the elastic constant, the volume for the piezoelectric constant was calculated by Eq. (2) and only one piezoelectric constant can be calculated, $e_{11}$.

The topological properties were evaluated by analyzing the critical points (CP) of the Zn-O, Ga-N, Zn-N and Ga-O bonds. These properties enable the unambiguous classification of chemical interactions. For the topological analyzes, the QTAIMAC [24] was employed through the TOPOND program [25], recently implemented to the CRYSTAL computational package.

A CP in the electron density, $\rho(\boldsymbol{r})$, is a point where the gradient of the density vanishes ($\nabla\rho(\boldsymbol{r}) = 0$). Each CP can be classified in terms of the eigenvalues, $\lambda_1$, $\lambda_2$, and $\lambda_3$ of the Hessian matrix; consequently, each CP can be labeled with two indices ($r$, $s$) where $r$ is the number of nonzero eigenvalues values and $s$ is the sum of the algebraic signs of the eigenvalues. Therefore, in particular case of the bond critical point

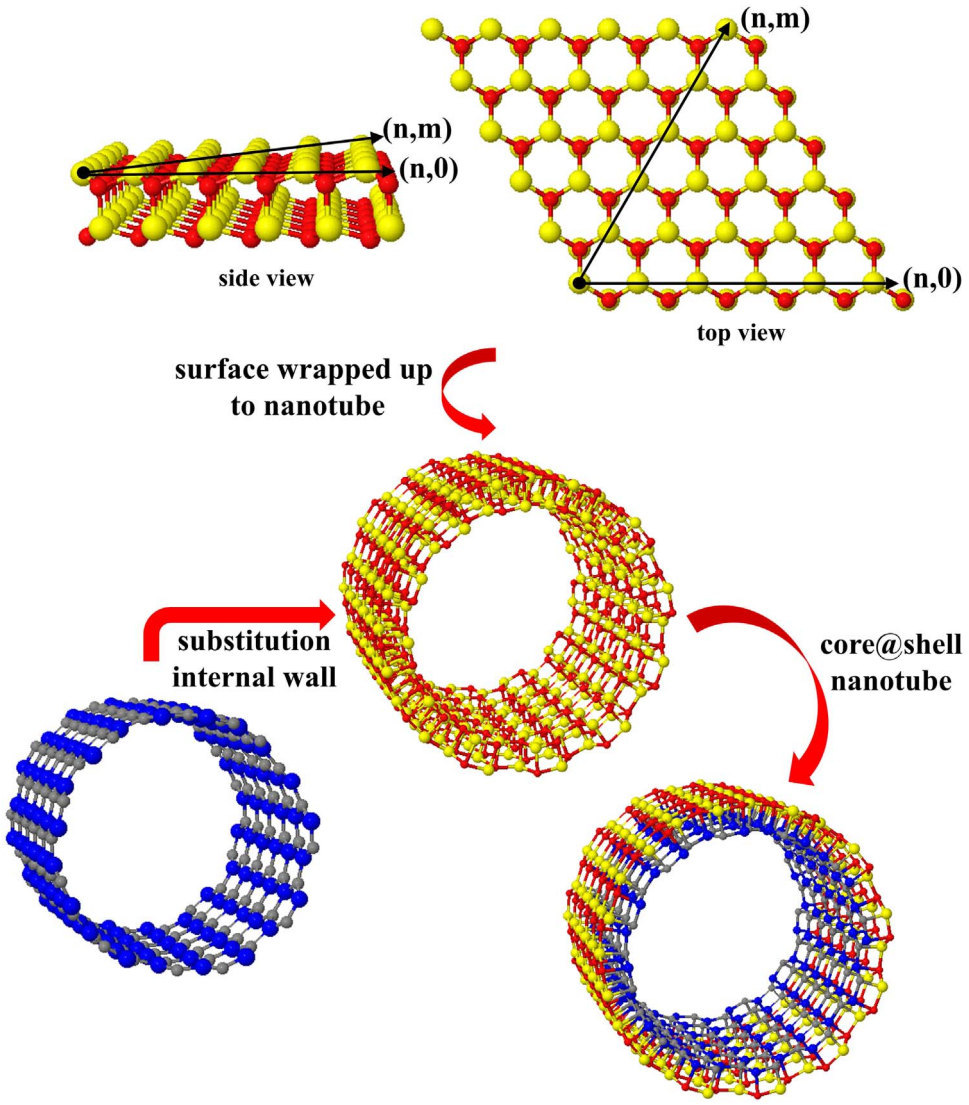


**Fig. 1.** Schematic representation of the core@shell nanotubes.

(BCP), (*r*, *s*) corresponding to (3, -1) and indicate a saddle point in the electron density scalar field, with a local minimum along the interatomic direction and two maxima in the perpendicular directions. Two topological properties of the charge in the vicinity of a BCP can be used to define the type of interaction between two (or more) atoms: the sign of the Laplacian of the electron density ($\nabla^2\rho(\boldsymbol{r})$) and the value of the potential to kinetic energy density ratio, $V(\boldsymbol{r})/T(\boldsymbol{r})$. Negative values of the Laplacian ($\nabla^2\rho(r) < 0$) and $V(\boldsymbol{r})/T(\boldsymbol{r}) > 2$ indicate charge accumulation in the BCP region, a characteristic of shared interactions and covalent bonds, whereas $\nabla^2\rho(r) > 0$ and $1 < V(\boldsymbol{r})/T(\boldsymbol{r}) < 2$ indicate charge depletion in the bond region and the prevalence of the kinetic energy with respect to the potential energy such as in ionic and hydrogen bonds and van der Waals interactions.

The ellipticity parameter (ε) gives a bond shape description, that is, how the electron density is "scattered" along the chemical bond. For a more scattered, non-directional density, the value obtained for ε is closer to 1, the bond shape is more elliptical, suggesting a bond with a more pronounced covalent character; in contrast, for a more concentrated density around one of the constituents of the bond, directional bond, the value obtained for ε is closer to 0, the bond shape is more cylindrical, suggesting a bond with a more pronounced ionic character.

The integration of the charge density over the atomic basins provides additional information, such as the atomic volume, Bader's atomic charge, and the atomic contributions in which the total energy of a system can be partitioned.

In this work, the BCPs have been determined using an eigenvector-following method, and Morse relationship [38] has been verified *a posteriori* for all structures.

The above discussion had as objective to introduce the reader to computational methods, especially DFT, applied to the solid state.

For details about the accuracy and implementation of elastic and piezoelectric and QTAIMAC, calculations with the CRYSTAL program, see Refs. [24–26,39–42] respectively.

## 3. Computational models

The thermodynamically stable phase of ZnO [43] and GaN [44] under normal conditions is the hexagonal wurtzite structure ($P6_3mc$ space group), which has two external parameters, $a$ (3.258 Å (ZnO) and 3.203 Å (GaN)) and $c$ (5.220 Å (ZnO) and 5.204 Å (GaN)), and one internal coordinate $u$ (0.382 (ZnO) and 0.377 (GaN)).

First, to determinate the bulk equilibrium structure of ZnO and GaN, their total energies were optimized with respect to the lattice parameters and the internal coordinate.

The previous calculated optimized bulk ZnO parameters [33] are $a$ = 3.274 Å, $c$ = 5.250 Å, and $u$ = 0.383, and are in agreement with other experimental and theoretical values [42,43,45,46]. The optimized lattice parameters for bulk GaN are $a$ = 3.209 Å, $c$ = 5.207 Å, and $u$ =

0.381, which show a deviation of 0.19%, 0.05%, and 0.10%, respectively, from experimental values [44].

In the second step, double-layer surfaces of ZnO and GaN (0001) were constructed from the optimized bulk structures and re-optimized with regard to their atomic positions and cell parameters.

On CRYSTAL program, the nanotubes are generated according to the Hamada indexes, $n$ and $m$, and represent the rolling vectors. Depending on the direction of the rolling surface, the nanotubes can be classified as armchair ($n$, $n$), zigzag ($n$, 0), and chiral nanotubes ($n$, $m$), where the integers $n$ and $m$ determine the diameter and chirality of the nanotube. The number of atoms ($n_{at}$) in a double-walled nanotube can be determined by $2\times[4(n^2 + nm + m^2).\ gcd^{-1}(2n + m, 2m + n)]$ while its structure is determined by means of the chiral vector $\vec{R} = n\vec{a}_1 + m\vec{a}_2$ in the unrolled sheet, where $\vec{a}_1$ and $\vec{a}_2$ are base vectors. In addition, the chiral nanotube angle ($\theta$) is defined as the angle between the $\vec{R}$ and $\vec{a}_1$ vectors. From $\vec{R}$, the nanotube diameter (D) and $\theta$ can be calculated as $D = \sqrt{3}\, d\frac{\sqrt{n^2 + nm + m^2}}{\pi}$ and $\theta = tan^{-1}\left(\sqrt{3}\frac{m}{2n+m}\right)$, respectively. For armchair nanotube the chiral angle $\theta$ is 30 degrees and for zigzag nanotube is zero degree.

According to a previous work [32,33], the nanotubes present conversion on strain and formation energies from ~ 20 Å of diameter. In this sense, two homogenous DW nanotubes, armchair (12, 12) and zigzag (20, 0), were constructed from the relaxed double-layer surfaces of ZnO and GaN and were fully optimized.

From the optimized homogenous DW nanotubes, the zigzag and armchair ZnO@GaN and GaN@ZnO nanotubes were built by substituting the internal wall with the second material. To generate the ZnO@GaN nanotubes, the DW GaN nanotubes had the internal wall replaced by ZnO; and to generate the GaN@ZnO nanotubes, the DW ZnO nanotubes had the internal wall replaced by GaN. The four core@shell structures obtained were re-optimized. Fig. 1 is a schematic representation of the core@shell nanotubes.

It is important to emphasize that the main objective is to represent the interactions, i.e., the chemical bonds, between the two core@shell nanotube models with 50at% of ZnO and GaN.

One of the most useful quantities to measure the stability of nanotubes is the strain energy ($E_s$). This quantity is the energy necessary to rolled-up a nanotube from a surface. Lower values indicate easy nanotube formation. The strain energy is calculated by $E_s = (E_{NT}/n_{NT}) - E_{ZnO@GaN(0001)}$, where $E_{NT}$ is the total energy of the optimized DW nanotube, $n_{NT}$ is the number of units in the nanotube, and $E_{ZnO@GaN(0001)}$ is the total energy of the (0001) surface of ZnO@GaN. For the homogenous DW nanotubes, the term $E_{ZnO@GaN(0001)}$ is replaced by $E_{GaN(0001)}$ or $E_{ZnO(0001)}$ for the GaN and ZnO nanotubes, respectively.

In order to characterize the interaction between GaN and ZnO, the deposition energies ($E_{dep}$) were calculated according to the equation:

$$E_{dep} = \frac{E_X - E_{GaN} - E_{ZnO}}{2S} \quad (5)$$

where $E_X$ corresponds to core@shell energy, the $E_{GaN}$ and $E_{ZnO}$ are the energies of the two separated moieties frozen in the minimum core@shell configuration, and $S$ is the nanotube area.

## 4. Results and discussion

The structural properties of the homogenous DW and core@shell nanotubes are discussed with respect to the nanotube diameter, average bond length, and bond angle, as showed in Table 1.

The homogenous DW nanotubes maintain the geometrical characteristics of the correspondent single-walled nanotubes, with an average Zn-O and Ga-N bond length of 1.99 Å and Zn-O-Zn and Ga-N-Ga bond angle of ~ 127° [32,33]. Both the armchair and zigzag configurations of the DW GaN nanotubes present diameters slightly higher (by ~ 0.47 Å and 0.01 Å, respectively) than the ZnO nanotubes. The bond length of the external walls of the optimized core@shell nanotubes is greater than that of their precursor, and the Zn-N bonds are slightly longer than the Ga-O bonds (by ~ 0.02 Å). Interestingly, owing to the higher diameter of the GaN nanotubes, the diameter of the structures in which GaN is in the core is higher than that of both the homogenous and ZnO@GaN structures.

**Table 1**
Diameter (D, Å), nanotube length ($l$, Å), average bond length (Å), angle (α, degrees), $E_s$ (eV/atom), $E_{dep}$ (eV/Å$^2$), and band gap energy ($E_{gap}$, eV) of the armchair and zigzag DW ZnO (DWZnONT), GaN (DWGaNNT), GaN@ZnO and ZnO@GaN nanotubes. The subindexes 1 and 2 refers to the internal and external wall, respectively.

| | DWZnONT | DWGaNNT | GaN@ZnO | ZnO@GaN |
|---|---|---|---|---|
| ***Armchair*** | | | | |
| **D** | 20.12 | 20.59 | 20.68 | 19.03 |
| ***l*** | 3.46 | 3.35 | 3.31 | 3.50 |
| **$Zn_1$-$O_1$** | 1.88 | – | – | 1.89 |
| **$Zn_2$-$O_2$** | 2.13 | – | 2.13 | – |
| **$Ga_1$-$N_1$** | – | 1.86 | 1.88 | – |
| **$Ga_2$-$N_2$** | – | 2.15 | – | 2.06 |
| **Zn-N** | – | – | 2.17 | 2.20 |
| **Ga-O** | – | – | 2.15 | 2.17 |
| $\alpha_{O\text{-}Zn\text{-}O}$ | 133.82 | – | 124.83 | 108.88 |
| $\alpha_{N\text{-}Ga\text{-}N}$ | – | 127.80 | 117.89 | 119.73 |
| $E_s$ | – 0.34 | 0.17 | – 0.31 | 0.00 |
| $E_{dep}$ | – | – | – 0.069 | – 0.055 |
| $E_{gap}$ | 3.49 | 2.94 | 3.59 | 2.91 |
| ***Zigzag*** | | | | |
| **D** | 19.72 | 19.73 | 20.26 | 18.90 |
| ***l*** | 5.91 | 5.75 | 5.69 | 5.95 |
| **$Zn_1$-$O_1$** | 1.88 | – | – | 1.86 |
| **$Zn_2$-$O_2$** | 2.11 | – | 2.10 | – |
| **$Ga_1$-$N_1$** | – | 1.87 | 1.88 | – |
| **$Ga_2$-$N_2$** | – | 2.09 | – | 2.07 |
| **Zn-N** | – | – | 2.17 | 2.18 |
| **Ga-O** | – | – | 2.14 | 2.15 |
| $\alpha_{O\text{-}Zn\text{-}O}$ | 124.60 | – | 131.90 | 105.04 |
| $\alpha_{N\text{-}Ga\text{-}N}$ | 126.48 | – | 117.16 | 122.62 |
| $E_s$ | – 0.33 | 0.01 | – 0.31 | 0.04 |
| $E_{dep}$ | – | – | – 0.069 | – 0.056 |
| $E_{gap}$ | 3.36 | 2.84 | 3.61 | 2.74 |

The strain energy $E_s$ (Table 1) of the armchair and zigzag DW ZnO nanotubes are lower and almost similar, which suggests that both configurations can be easily formed. In a previous work about single-walled ZnO nanotubes, the armchair and zigzag nanotubes present also the same $E_s$ [32]. Comparing the $E_s$ of DW nanotubes with the respective single-walled nanotubes, the $E_s$ of DW is almost 0.01 eV/atom lower than single-walled nanotubes, indicating that the DW is probably slightly easier to form than single-walled. From an experimental point of view, multi-walled nanotubes are more easily synthesized than single-walled nanotubes because the synthesis of the latter requires stricter and more controlled procedures. This accounts for the higher proportion of published experimental papers related to multi-walled nanotubes than single-walled nanotubes.

The $E_s$ of the zigzag DW GaN nanotube is slightly lower than that of the armchair nanotube (~ 0.16 eV/atom). In general, based on the $E_s$ values, the DW ZnO nanotubes can be more easily obtained than the DW GaN and core@shell nanotubes, although GaN@ZnO presents $E_s$ values very close to that of the ZnO nanotubes (the difference is ~ 0.02 eV/atom).

For both armchair and zigzag configurations, the core@shell formation leads to high $E_s$ when the shell consists of GaN. The GaN@ZnO nanotubes present the lowest $E_s$ of about – 0.31 eV/atom; therefore, these nanotubes can be more easily formed than ZnO@GaN.

In order to predict the more favorable core@shell combination, and the better choice of the material to be used as a substrate in a deposition (or coating), the deposition energy was calculated and showed that the both GaN@ZnO nanotubes are the ones with the

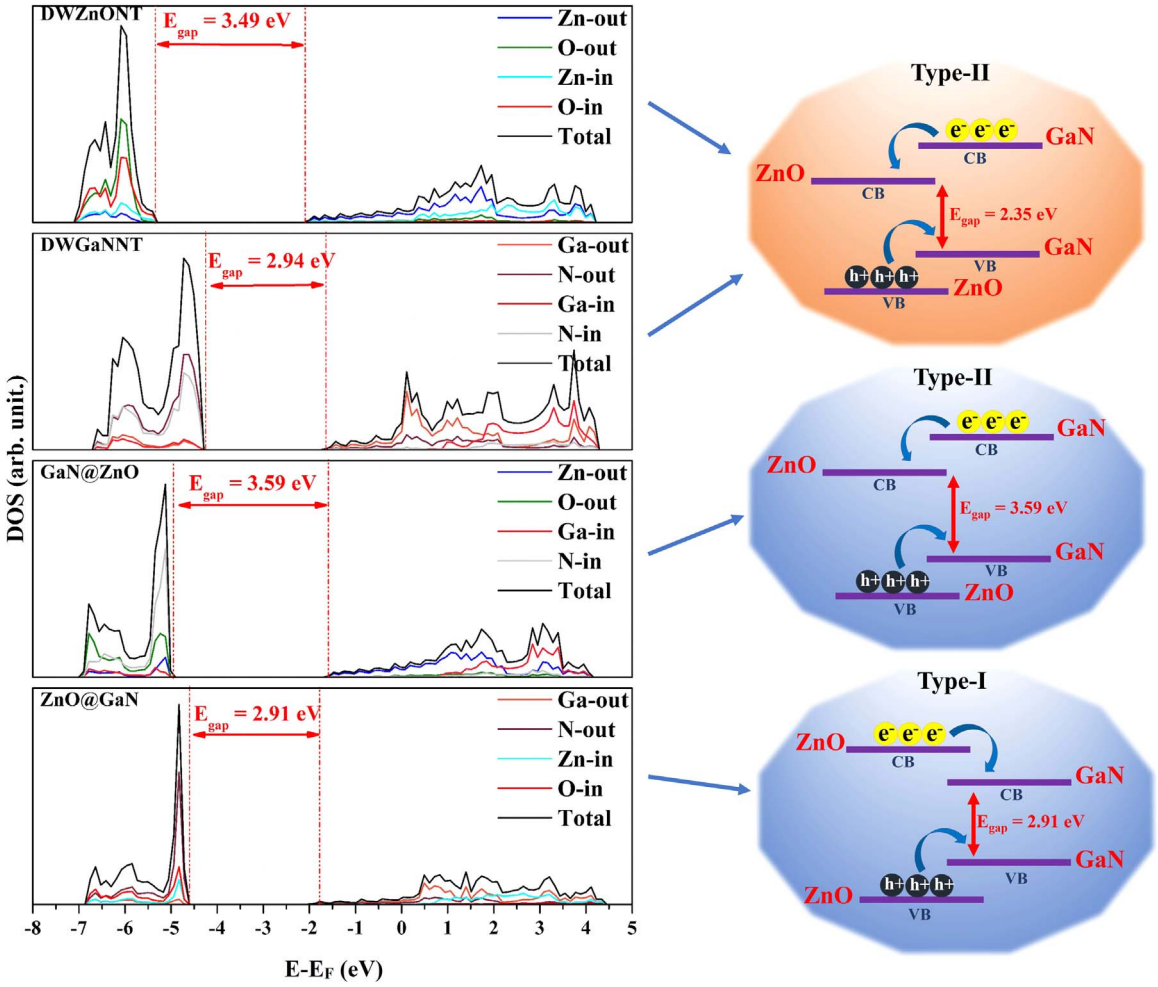


**Fig. 2.** Total density of states and electron-hole pairs of armchair nanotubes. The labels in and out refers to the internal and outer of nanotube wall.

lowest energy, with about 19% higher than ZnO@GaN.

In particular, the relative stability between the two core@shell systems is estimated to be around 0.30 eV/atom per cell for $E_s$ and 0.013 eV/Å$^2$ for $E_{dep}$. Based on purely energetic considerations, GaN@ZnO is the most promising core@shell nanotube. The stability of core@shell nanotubes can be explained in terms of two effects: i) the strain imposed on the layer to wrap it and ii) the formation of new bonds between the two different wall materials. As evidenced by the bond lengths and bond angles in Table 1, the external wall undergoes a greater deformation.

It is known that electronic conduction in nanotubes occurs in a spiral through the nanotube wall [47], and therefore the band gap is directly related to the composition of the wall. The band gap of homogeneous nanotubes, such as ZnO and GaN, is very close to the band gap calculated for the corresponding monolayer surfaces. By increasing the number of layers and consequently the wall thickness, the band gap is reduced and tends towards the bulk-like value.

According to the aforementioned, the core@shell nanotubes will have band gaps similar to that of the material that forms the external wall. Therefore, the $E_{gap}$ of ZnO@GaN is lower than that of GaN@ZnO by 0.68 eV for the armchair and 0.87 eV for the zigzag nanotube. However, both the homogeneous DW and core@shell nanotubes retain a semiconductor character and consequently their potential applicability in electronic devices.

Based on the $E_{gap}$, both the armchair and zigzag configurations of the ZnO and GaN@ZnO nanotubes exhibit absorption at near UV region (UVA, ~315–380 nm), while the GaN and ZnO@GaN nanotubes, it appears at visible region, with the armchair nanotube in the violet range (~ 380–435 nm) and the zigzag in the blue range (~ 435–500 nm). These data are in agreement with other theoretical results [19,20]. Therefore, the absorption region of the nanotubes does not only depend on the chemical composition of the outer layer but also on the configuration of the nanotube, which therefore become a determining factor for their application in LEDs of different colors. Furthermore, a shift in the region of the electromagnetic spectrum from UVA to visible light opens the possibility to employ ZnO@GaN nanotubes in solar cells and other energy-harvesting devices.

Hong and co-workers experimentally obtained ZnO@GaN nanotubes with a ZnO internal wall and showed that the band gap ranged from 3.0 to 3.6 eV [7]; therefore, the absorption of the nanotube shifts from the UVA to the violet region. By comparing our calculated band gap of 2.91 eV for ZnO@GaN, which corresponds to the violet range, with the results obtained by Hong, it is possible to assign the armchair configuration to his structures.

The band structures (Figs. S1 and S2) of the homogenous and core@shell nanotubes show a direct band gap at the Γ point, except for the armchair configuration of GaN and ZnO@GaN, which is characterized by an indirect band gap between the Γ-X points. On both core@shell band structures, the bands of the chilarities are flat and concentrated around the top of the valence band (VB), which means that the electrons have low mobility in this region; while on conduction band (CB), the bands are more scattered and non-flat, indicating a good dispersion and a higher mobility for the electrons. This result is in agreement with the findings of Lim et al. [19], who revealed an indirect band gap for Zn and O co-doped GaN nanotubes and ascribed this shift to the concentration of ZnO. In our opinion, the difference is due to the

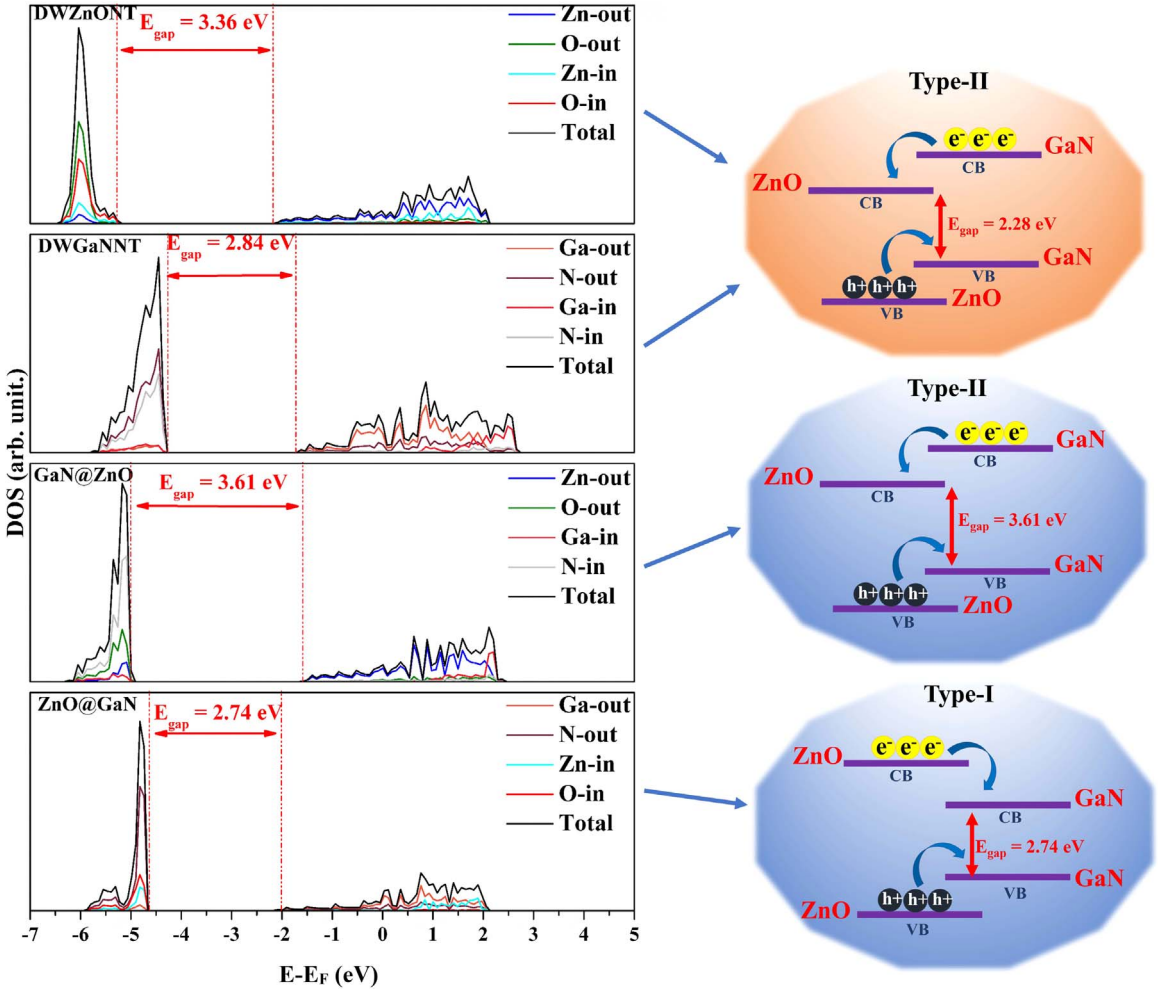


**Fig. 3.** Total density of states and electron-hole pairs of zigzag nanotubes. The labels in and out refers to the internal and outer of nanotube wall.

arrangement of atoms in the armchair nanotubes in addition to the Ga and N atoms forming the outer layer of the nanotube because the GaN armchair nanotube also presents an indirect gap.

Core@shell structures present peculiar interfacial features that can be useful to improve the chemical and physical properties of new materials for widespread applications [48–53]. One of the most useful approaches to evaluate electronic transitions in core@shell models is the band alignment. This method consists of analyzing the top valence and bottom conduction band energies of the core and shell materials. Accordingly, the core@shell structures can be classified as type-I and/or type-II behavior, depending on the band offset between the two materials [54,55]. The ZnO@GaN and GaN@ZnO structures usually exhibit type-II behavior provided by band alignment [11,12].

However, although band alignment is widely used to predict the electronic transition type in core@shell systems, this method analyses the two moieties separately, which can lead to hasty conclusions. In the present work, it is proposed the analysis of the electronic transition and the interface type taking into account the bonds formed between the core and the shell. In this sense, the electron transfer in the core@shell nanotubes was analyzed using DOS projected on the atoms of each wall (Figs. 2 and 3) and on the atomic orbitals of each atom (Figs. S3 and S4). Thus, the atom with the highest density of states in VB will be considered as the atom that the electron will “leave” in VB and the one with the highest density of states in the CB will be considered as the atom that will "receive" the electron after the VB-CB transition. If both atoms belong to the same material, for example VB-N and CB-Ga, it will be considered type-I; if they belong to different materials, for example, VB-N and CB-Zn, it will be considered type-II.

As seen in Figs. 2 and 3, both the armchair and zigzag nanotubes exhibit a type-II behavior by band alignment, and the effective $E_{gap}$ are 2.35 eV and 2.28, respectively. The electronic transition can be considered to occur from the VB of GaN to the CB of ZnO. Taking to account the orbitals that present the major contribution to the top and bottom of the VB and CB, respectively, of DW ZnO and DW GaN nanotubes, the electronic transition of the core@shell occurs when the electron in the O-2p is promoted to the N-2p, creating a hole in the oxygen VB. Whit a minimum excitation correspondent to the band gap, the electron on nitrogen will be promoted to Zn-s, and finally to Ga-s. The formed hole follows an opposite path. When the electron loses energy and returns to its ground state, recombination of the electron-hole pair occurs.

Both, the band alignment and DOS, showed that GaN@ZnO nanotubes presents type-II behavior for the interface, and the transition occurs between the N atoms of VB and the Zn atoms of CB. In contrast to that observed with the band alignment, for the ZnO@GaN nanotubes, the behavior of interface observed by the DOS analysis is type-I, with the transition occurring between N atoms in VB and Ga atoms in CB. Therefore, the atoms that constitute the outer wall of the core@shell nanotubes have a great influence on the electronic properties, as observed for the pure ZnO and GaN nanotubes. The orbitals that most contribute on VB are N-$2p_xp_y$, O-$2p_xp_y$, Ga-$2p_xp_y$, and Zn-$3d_{x^2}$-$y^2$ and on CB are Zn-s and Ga-s. Thus, these results show that electronic conduction occurs on the external wall and confirm the crucial influence of the nature of the external wall.

Table 2 presents the elastic and piezoelectric constants of the homogeneous and core@shell nanotubes. Direct comparison of the

**Table 2**
Elastic (GPa) and piezoelectric ($C\,m^{-2}$) constants of the armchair and zigzag nanotubes.

| | ZnO | GaN | GaN@ZnO | ZnO@GaN |
|---|---|---|---|---|
| ***Armchair*** | | | | |
| $C_{11}$ | 261.26 | 475.78 | 392.80 | 291.26 |
| $e_{11}$ | – | – | – | – |
| ***Zigzag*** | | | | |
| $C_{11}$ | 291.41 | 476.79 | 371.44 | 394.20 |
| $e_{11}$ | − 0.62 | − 0.18 | 0.40 | − 1.45 |

elastic constants shows that the GaN nanotubes are more rigid than the ZnO nanotubes. The difference observed for the elastic constants of homogenous DW nanotubes can be related to the strain and deposition energies of the core@shell nanotubes. In the GaN@ZnO nanotubes, the ZnO outer wall can relax its structure to "receive" the GaN (which has a higher diameter than ZnO). On the other hand, the lower elasticity of GaN does not allow for enough expansion to "accommodate" ZnO. Thus, the stability of the GaN@ZnO nanotubes can be derived from the greater elasticity of the outer wall.

However, for both the homogeneous ZnO and GaN nanotubes, the zigzag configuration is more rigid than the armchair. For the core@shell nanotubes, the elastic constants not only depend on the composition of the external wall, but also on the chirality of the nanotube. The armchair GaN@ZnO nanotube is 25.85% more rigid than the armchair ZnO@GaN nanotube but the zigzag ZnO@GaN nanotube is 5.77% more rigid than the zigzag GaN@ZnO nanotube.

According to our results, the armchair nanotubes do not present any piezoelectric behavior, and this is in agreement with the predictions of Sai and Tu [55,56]. Therefore, a piezoelectric response occurs only in the zigzag nanotubes. The DW ZnO nanotube shows a piezoelectric response 3.44 times higher than the DW GaN nanotube, and this behavior leads to a higher piezoelectric response in the ZnO@GaN core@shell nanotube. In this case, the inner wall seems to provide the main contribution to the piezoelectric response; thus, ZnO@GaN exhibits the best performance although GaN@ZnO has a higher modulus piezoelectric response than GaN.

The nanotube length of the ZnO@GaN is 5.95 Å, which is 0.04 Å and 0.21 Å greater than ZnO and GaN nanotubes, respectively, meaning that GaN is under strain in the core@shell system. In order to prove that the elongation leads to the increase in the piezoelectric constants, the simulation of the strain along the periodic direction (nanotube length) of the major piezoelectric nanotube, ZnO@GaN, were made. The strain applied take into account the variation of ± 4%. It was observed that the compression maintains the piezoelectric response on 1.45 C. $m^{-2}$, while the elongation increases the piezoelectric on ~ 12% (1.62 C $m^{-2}$), which indicates significant influence of the positive stress on the piezoelectric response.

In the particular case of GaN@ZnO nanotubes, these nanotubes are easier obtained then ZnO@GaN, in contrast, presents the highest band gap energy and the minor piezoelectric response. Applying strain on nanotube can be considered a way to increment its piezoelectric performance and the same time lead a band gap modification. Therefore, when the strain is applied (Table S1), there is a significant increase in the piezoelectric response and, in contrast, there is a decrease in the band gap value. The increase in piezoelectricity can reach 317% (1.67 C $m^{-2}$) when the applied strain is 10%, obtaining a piezoelectric response higher than the ZnO@GaN nanotube and ZnO and GaN bulk. In addition, by applying 6% strain, the emission range of the electromagnetic spectrum becomes violet, due to the band gap reduction to 3.40 eV, and with 10% change to the blue region. Therefore, under strain, the material can also be used in solar cells and other energy-harvesting devices.

It is noteworthy that, although there is a reduction of the nanotube diameters and stretching of the bond distances, there is no rupture on its structure. Moreover, both, ZnO@GaN and GaN@ZnO, presented increased on the piezoelectric response and reduction on $E_{gap}$ when strain is applied, however, due to the greater malleability of the GaN@ZnO, the influence of strain on its properties is greater. Interesting enough, the GaN@ZnO improved the piezoelectricity response until + 10%, which did not occur for ZnO@GaN that had a huge decrease on piezoelectricity response from −2.29 C $m^{-2}$ (for 8% strain) to 0.09 C $m^{-2}$. The decrease on piezoelectricity response for GaN@ZnO occurred with + 15% of elongation (Table S1).

Finally, the topological properties of the nanotubes have been calculated and are shown in Table 3. The BCPs for all nanotubes

**Table 3**
Topological analysis of the electronic density ($\rho(r)$), Laplacian ($\nabla^2\rho$), |V|/G ratio, bond degree (H/ $\rho(r)$), and Bader bond charge (BC) of the homogenous and core@shell nanotubes. Values are in atomic units and distances between critical points and atoms ($d_{PC-X}$) are in Å. The sub-indexes 1 and 2 refers to the internal and external wall, respectively.

| | ZnO | | GaN | | GaN@ZnO | | | | ZnO@GaN | | | |
|---|---|---|---|---|---|---|---|---|---|---|---|---|
| | **Zn-O** | **$Zn_1$-$O_2$** | **Ga-N** | **$Ga_1$-$N_2$** | **$Ga_1$-$N_1$** | **$Ga_1$-$O_2$** | **$Zn_2$-$N_1$** | **$Zn_2$-$O_2$** | **$Zn_1$-$O_1$** | **$Zn_1$-$N_2$** | **$Ga_2$-$O_1$** | **$Ga_2$-$N_2$** |
| ***Armchair*** | | | | | | | | | | | | |
| $d_{PC-Zn}$ | 0.92 | 1.02 | – | – | – | – | 1.03 | 1.02 | 0.92 | 1.04 | – | – |
| $d_{PC-O}$ | 0.97 | 1.11 | – | – | – | 1.13 | – | 1.11 | 0.97 | – | 1.14 | – |
| $d_{PC-Ga}$ | – | – | 0.88 | 0.95 | 0.90 | 1.02 | – | – | – | – | 1.02 | 0.98 |
| $d_{PC-N}$ | – | – | 0.95 | 1.04 | 0.97 | – | 1.15 | – | – | 1.16 | – | 1.08 |
| $\rho$ | 0.10 | 0.06 | 0.13 | 0.09 | 0.14 | 0.06 | 0.06 | 0.08 | 0.10 | 0.06 | 0.06 | 0.08 |
| $\nabla^2\rho$ | 0.61 | 0.24 | 0.53 | 0.26 | 0.43 | 0.20 | 0.20 | 0.37 | 0.06 | 0.18 | 0.18 | 0.18 |
| **V/G** | 1.06 | 1.09 | 1.20 | 1.29 | 1.22 | 1.19 | 1.23 | 1.06 | 1.06 | 1.24 | 1.19 | 1.35 |
| **H/$\rho$** | − 0.09 | − 0.11 | − 0.26 | − 0.29 | − 0.22 | − 0.19 | − 0.22 | − 0.11 | − 0.09 | − 0.24 | − 0.18 | − 0.28 |
| **$\varepsilon$** | 0.01 | 0.02 | 0.04 | 0.07 | 0.04 | 0.01 | 0.02 | 0.02 | 0.01 | 0.01 | 0.01 | 0.07 |
| **BC** | 0.0 | 0.15 | 0.0 | 0.15 | 0.05 | 0.09 | − 0.09 | − 0.05 | − 0.04 | − 0.41 | 0.42 | 0.05 |
| ***Zigzag*** | | | | | | | | | | | | |
| | **Zn-O** | **$Zn_1$-$O_2$** | **Ga-N** | **$Ga_1$-$N_2$** | **$Ga_1$-$N_1$** | **$Ga_1$-$O_2$** | **$Zn_2$-$N_1$** | **$Zn_2$-$O_2$** | **$Zn_1$-$O_1$** | **$Zn_1$-$N_2$** | **$Ga_2$-$O_1$** | **$Ga_2$-$N_2$** |
| $d_{PC-Zn}$ | 0.92 | 1.01 | – | – | – | – | 1.02 | 1.01 | 0.91 | 1.03 | – | – |
| $d_{PC-O}$ | 0.97 | 1.10 | – | – | – | 1.01 | – | 1.09 | 0.95 | – | 1.13 | – |
| $d_{PC-Ga}$ | – | – | 0.90 | 0.99 | 0.90 | 1.13 | – | – | – | – | 1.02 | 0.99 |
| $d_{PC-N}$ | – | – | 0.97 | 1.09 | 0.98 | – | 1.14 | – | – | 1.15 | – | 1.09 |
| $\rho$ | 0.10 | 0.06 | 0.12 | 0.07 | 0.11 | 0.06 | 0.06 | 0.06 | 0.10 | 0.06 | 0.06 | 0.08 |
| $\nabla^2\rho$ | 0.62 | 0.26 | 0.44 | 0.17 | 0.42 | 0.20 | 0.20 | 0.27 | 0.67 | 0.19 | 0.20 | 0.16 |
| **V/G** | 1.06 | 1.09 | 1.21 | 1.36 | 1.22 | 1.19 | 1.22 | 1.09 | 1.06 | 1.23 | 1.19 | 1.36 |
| **H/$\rho$** | − 0.10 | − 0.10 | − 0.25 | − 0.29 | − 0.26 | − 0.19 | − 0.22 | − 0.10 | − 0.10 | − 0.23 | − 0.19 | − 0.28 |
| **$\varepsilon$** | 0.01 | 0.03 | 0.03 | 0.06 | 0.04 | 0.00 | 0.01 | 0.02 | 0.01 | 0.00 | 0.01 | 0.07 |
| **BC** | 0.0 | 0.17 | 0.0 | 0.17 | 0.06 | 0.08 | − 0.07 | − 0.05 | − 0.05 | − 0.43 | 0.43 | 0.05 |

analyzed are almost equidistant between the two nuclear attractors, being slightly closer to the metals ($d_{Pc-Zn}$ and $d_{Pc-Ga}$ are ~0.9 Å), suggesting a non-directionality of bonds. Besides that, the positive values of the Laplacian and positive BCP densities ($\rho$) around 0.1 e/bohr$^3$ suggest an ionic nature of the nanotubes bonds. The bond degree ($H/\rho$) of all analyzed bonds is almost zero, indicating a transitory bond type. In addition, the low ellipticity value ($\varepsilon$ is almost zero), highlights the cylindrically symmetric shape of the bonds and suggests a directional bond. Therefore, according to the topological analysis, the general description of the Zn-O, Ga-N, Zn-N and Ga-O bonds corresponds to the transitory region, i.e., neither ionic nor covalent. Nevertheless, on DW nanotubes, the Ga-N bonds are ~38% more covalent than the Zn-O bonds. The same behavior is observed for the core@shell nanotubes. The interface Zn-N bonds exhibit a more pronounced covalent character than the Ga-O bonds.

Regarding Bader charges for the DW nanotube bonds, the bond charge of the inner wall is taken to zero and the second wall shows the bond charge difference between the outer and inner walls. The core@shell nanotube bonds were analyzed according to the difference between the bond charges of the core@shell nanotubes and the correspondent bonds on DW nanotubes. The Bader charge analysis on the chemical bonds reveals that the DW ZnO and GaN nanotubes present an accumulated charge of ~0.17$e$ and 0.15$e$ on the external wall for the armchair and zigzag configuration, respectively, indicating that the charges flow from the internal to the external wall. In contrast, the core@shell nanotubes present a charge flow from the GaN wall to the ZnO wall, regardless of their core or shell nature, and the charges are concentrated on the interfacial Zn-N bonds, a result that is also confirmed by the high electronic density. The electron accumulation on the ZnO wall allows for electrons and holes to be spatially separated and thus hinders electron-hole recombination. Such core@shell nanotubes can therefore be employed in solar cells.

## 5. Conclusions

The main objective of this work was to describe the properties of ZnO@GaN and GaN@ZnO core@shell nanotubes and predict the structure with the best performance as function of some specific properties to guide experimental synthesis and applications.

The evaluation of the structural and electronic features showed that properties were influenced by the nature of the external wall of the core@shell nanotubes.

For both chiralities, the strain and deposition energies show that GaN@ZnO can be more easily formed and GaN is a better substrate than ZnO. Besides that, the elastic constant shows that the stability of the GaN@ZnO core@shell nanotubes can be related to the higher elasticity of the ZnO nanotubes and the best possibility to “accommodate” the GaN nanotubes. Under strain, the nanotubes had a greater piezoelectric response and band gap reduction, which provides increased on their applications.

In terms of electronic properties, the GaN nanotubes exhibit lower band gap energy than the ZnO nanotubes, and consequently, the band gap energy of ZnO@GaN is lower than that of GaN@ZnO for both the armchair and zigzag configurations. Based on their band gap energy values, the ZnO and GaN@ZnO nanotubes exhibit absorption in the UVA region of the spectrum, while GaN and ZnO@GaN nanotubes show different absorptions that depend on their chirality, i.e., in the violet region for the armchair and in the blue region for the zigzag. However, it was showed that the nanotubes under elongation can be exhibit absorption in different region on the electromagnetic spectrum.

The DOS was crucial to explain the electronic transitions at the interface and to correctly predict the type of the core@shell structures. Therefore, the GaN@ZnO nanotubes exhibit type-II behavior, while ZnO@GaN exhibit type-I.

Finally, the Bader charge analysis shows that the charges flow from the GaN wall to the ZnO wall, independently of the core@shell nanotube, and there is a charge accumulation around Zn-N bonds. Also, all analyzed bonds belongs to a transitory region.

According to these results, ZnO@GaN and GaN@ZnO core@shell nanotubes can be both employed in many electronic devices and the zigzag nanotubes on piezoelectric devices.

## Acknowledgments

This work is supported by Brazilian Funding Agencies: CAPES PROCAD (8881.068492/2014-01 and 787027/2013), FAPESP (2016/07476-9, 2016/25500-4, and 2013/07296-2). The computational facilities were supported by resources supplied by Molecular Simulations Laboratory, São Paulo State University, Bauru, Brazil.

## Appendix A. Supplementary material

Supplementary data associated with this article can be found in the online version at doi:10.1016/j.jssc.2018.07.023.

## References

[1] T. Minami, H. Sato, H. Nanto, S. Takata, Group III impurity doped zinc oxide thin films prepared by RF magnetron sputtering, Jpn. J. Appl. Phys. 24 (1985) 781–L784.
[2] F. Bernardini, V. Fiorentini, Spontaneous versus piezoelectric polarization in III ± V nitrides: conceptual aspects and practical consequences, Phys. Status Solidi 216 (1999) 391–398.
[3] O. Ambacher, J. Smart, J.R. Shealy, N.G. Weimann, K. Chu, M. Murphy, W.J. Schaff, L.F. Eastman, R. Dimitrov, L. Wittmer, M. Stutzmann, W. Rieger, J. Hilsenbeck, Two-dimensional electron gases induced by spontaneous and piezoelectric polarization charges in N- and Ga-face AlGaN/GaN heterostructures, J. Appl. Phys. 85 (1999) 3222–3233.
[4] R. Li, P.I. Reyes, S. Ragavendiran, H. Shen, Y. Lu, Tunable surface acoustic wave device based on acoustoelectric interaction in ZnO/GaN heterostructures, Appl. Phys. Lett. 107 (2015) (073504–073504-5).
[5] S. Jeong, H. Kim, Enhanced performance characteristics of n-ZnO/p-GaN heterojunction light-emitting diodes by forming excellent Ohmic contact to p-GaN, Mater. Sci. Semicond. Process. 39 (2015) 771–774.
[6] K. Maeda, T. Takata, M. Hara, N. Saito, Y. Inoue, H. Kobayashi, K. Domen, GaN:ZnO solid solution as a photocatalyst for visible-light-driven overall water splitting, J. Am. Chem. Soc. 127 (2005) 8286–8287.
[7] Y.J. Hong, J.M. Jeon, M. Kim, S.R. Jeon, K.H. Park, G.C. Yi, Structural and optical characteristics of GaN/ZnO coaxial nanotube heterostructure arrays for light-emitting device applications, New J. Phys. 11 (2009) (125021– 125021-13).
[8] J.R. Sadaf, M.Q. Israr, S. Kishwar, O. Nur, M. Willander, White electroluminescence using ZnO nanotubes/GaN heterostructure light-emitting diode, Nanoscale Res. Lett. 5 (2010) 957–960.
[9] M. Law, J. Goldberger, P. Yang, Semiconductor nanowires and nanotubes, Annu. Rev. Mater. Res. 34 (2004) 83–122.
[10] L. Zhang, Q. Li, L. Shang, Z. Zhang, R. Huang, F. Zhao, Electroluminescence from n-ZnO:Ga/p-GaN heterojunction light-emitting diodes with different interfacial layers, J. Phys. D: Appl. Phys. 45 (2012) (485103– 485103-6).
[11] J.W. Sun, Y.M. Lu, Y.C. Liu, D.Z. Shen, Z.Z. Zhang, B.H. Li, J.Y. Zhang, B. Yao, D.X. Zhao, X.W. Fan, Excitonic electroluminescence from ZnO-based heterojunction light emitting diodes, J. Phys. D: Appl. Phys. 41 (2008) (155103–155103-5).
[12] M.N. Huda, Y. Yan, S.H. Wei, M.M. Al-Jassim, Electronic structure of ZnO:GaN compounds: asymmetric bandgap engineering, Phys. Rev. B - Condens. Matter Mater. Phys. 78 (2008) (195204–195204-5).
[13] L. Li, J.T. Muckerman, M.S. Hybertsen, P.B. Allen, Phase diagram, structure, and electronic properties of (Ga 1–xZn x)(N 1–xO x) solid solutions from DFT-based simulations, Phys. Rev. B 83 (2011) 134202–134206.
[14] A.A. Reinert, C. Payne, L. Wang, J. Ciston, Y. Zhu, P.G. Khalifah, Synthesis and characterization of visible light absorbing (GaN)1–x(ZnO)x semiconductor nanorods, Inorg. Chem. 52 (2013) 8389–8398.
[15] J. Lei, D.P. Zhu, M.C. Xu, S.J. Hu, First-principles simulations of two dimensional electron gas near the interface of ZnO/GaN (0001) superlattice, Phys. Lett. A 379 (2015) 2384–2387.
[16] H. Zhang, C. Xia, X. Tan, T. Wang, S. Wei, Effects of polar and nonpolar on band structures in ultrathin ZnO/GaN type-II superlattices, Solid State Commun. 221 (2015) 14–17.
[17] H. Pan, Y.W. Zhang, GaN/ZnO superlattice nanowires as photocatalyst for hydrogen generation: a first-principles study on electronic and magnetic properties, Nano Energy 1 (2012) 488–493.
[18] Y. Zhang, D.-Q. Fang, S.-L. Zhang, R. Huang, Y.-H. Wen, Structural and electronic properties of ZnO/GaN heterostructured nanowires from first-principles study, Phys. Chem. Chem. Phys. 18 (2016) 3097–3102.
[19] Y.K. Lim, E.W. Keong Koh, Y.W. Zhang, H. Pan, Ab initio design of GaN-based photocatalyst: zno-codoped GaN nanotubes, J. Power Sources 232 (2013) 323–331.

[20] G.-L. Chai, C.-S. Lin, W.-D. Cheng, Graphitic GaN–ZnO and corresponding nanotubes, J. Mater. Chem. 21 (2011) 17071–17076.
[21] M.A. Abbasi, Z.H. Ibupoto, M. Hussain, O. Nur, M. Willander, The fabrication of white light-emitting diodes using the n-ZnO/NiO/p-GaN heterojunction with enhanced luminescence, Nanoscale Res. Lett. 8 (2013) 1–6.
[22] N.H. Alvi, K. ul Hasan, O. Nur, M. Willander, The origin of the red emission in n-zno nanotubes/p-gan white light emitting diodes, Nanoscale Res. Lett. 6 (2011) 1–7.
[23] C.H. Lee, Y.J. Hong, Y.J. Kim, J. Yoo, H. Baek, S.R. Jeon, S.J. Lee, G.C. Yi, GaN/ZnO nanotube heterostructure light-emitting diodes fabricated on Si, IEEE J. Sel. Top. Quant. Elec. 17 (2011) 966–970.
[24] R.F.W. Bader, Atoms in Molecules: A Quantum Theory, 1990.
[25] C. Gatti, Chemical bonding in crystals: new directions, Z. Krist. 220 (2005) 399–457.
[26] R. Dovesi, R. Orlando, A. Erba, C.M. Zicovich-Wilson, B. Civalleri, S. Casassa, L. Maschio, M. Ferrabone, M. De La Pierre, P. D'Arco, Y. Noël, M. Causà, M. Rérat, B. Kirtman, CRYSTAL14: a program for the ab initio investigation of crystalline solids, Int. J. Quantum Chem. 114 (2014) 1287–1317.
[27] A.D. Becke, Density functional thermochemistry. 3. The role of the exact exchange, J. Chem. Phys. 98 (1993) 5648–5652.
[28] J.E. Jaffe, A.C. Hess, Hartree-Fock study of phase changes in ZnO at high pressure, Phys. Rev. B 48 (1993) 7903–7909.
[29] T. Bredow, K. Jug, R.A. Evarestov, Electronic and magnetic structure of ScMnO3, Phys. Status Solidi B 243 (2006) R10–R12.
[30] R. Pandey, J.E. Jaffe, N.M. Harrison, Ab initio study of high pressure phase transition in GaN, J. Phys. Chem. Solids 55 (1994) 1357–1361.
[31] R. Dovesi, M. Causa, R. Orlando, C. Roetti, V.R. Saunders, Ab initio approach to molecular crystals: a periodic Hartree–Fock study of crystalline urea, J. Chem. Phys. 92 (1990) 7402–7411.
[32] N.L. Marana, S. Casassa, E. Longo, J.R. Sambrano, Structural, electronic, vibrational, and topological analysis of single-walled zinc oxide nanotubes, J. Phys. Chem. C 120 (2016) 6814–6823.
[33] N.L. Marana, A.R. Albuquerque, F.A. La Porta, E. Longo, J.R. Sambrano, Periodic density functional theory study of structural and electronic properties of single-walled zinc oxide and carbon nanotubes, J. Solid State Chem. 237 (2016) 36–47.
[34] N.L. Marana, S.M. Casassa, J.R. Sambrano, Piezoelectric, elastic, Infrared and Raman behavior of ZnO wurtzite under pressure from periodic DFT calculations, Chem. Phys. 485–486 (2017) 98–107.
[35] N.L. Marana, S.M. Casassa, J.R. Sambrano, Adsorption of NH3 with Different coverages on single-walled ZnO nanotube: DFT and QTAIM study, J. Phys. Chem. C 121 (2017) 8109–8119.
[36] M.C. Mazini, J.R. Sambrano, A.A. Cavalheiro, D.M. Gonçalves Leite, J.H.D. Da Silva, Efeitos da adição de átomos de mn na rede do gan via métodos de estrutura eletrônica, Quím. Nova. 33 (2010) 834–840.
[37] G.S.L. Fabris, N.L. Marana, E. Longo, J.R. Sambrano, Theoretical study of porous surfaces derived from graphene and boron nitride, J. Solid State Chem. 258 (2018) 247–255.
[38] P.L.A. Popelier, A robust algorithm to locate automatically all types of critical points in the charge density and its Laplacian, Chem. Phys. Lett. 228 (1994) 160–164.
[39] W.F. Perger, J. Criswell, B. Civalleri, R. Dovesi, Ab-initio calculation of elastic constants of crystalline systems with the CRYSTAL code, Comput. Phys. Commun. 180 (2009) 1753–1759.
[40] A. Erba, K.E. El-Kelany, M. Ferrero, I. Baraille, M. Rérat, Piezoelectricity of SrTiO3: an ab initio description, Phys. Rev. B 88 (2013) (35102–035102-10).
[41] Y. Noël, C.M. Zicovich-Wilson, B. Civalleri, P. D'Arco, R. Dovesi, Polarization properties of ZnO and BeO: an ab initio study through the Berry phase and Wannier functions approaches, Phys. Rev. B 65 (2001) (14111–14111-9).
[42] M. Catti, Y. Noel, R. Dovesi, Full piezoelectric tensors of wurtzite and zinc blende ZnO and ZnS by first-principles calculations, J. Phys. Chem. Solids 64 (2003) 2183–2190.
[43] F. Decremps, F. Datchi, A.M. Saitta, A. Polian, S. Pascarelli, A. Di Cicco, J.P. Itié, F. Baudelet, Local structure of condensed zinc oxide, Phys. Rev. B 68 (2003) (104101–104101-10).
[44] J.H.D. da Silva, D.M.G. Leite, A. Tabata, A.A. Cavalheiro, Structural and vibrational analysis of nanocrystalline Ga1-xMnxN films deposited by reactive magnetron sputtering, J. Appl. Phys. 102 (2007) (63526–63526-6).
[45] Ü. Özgür, Y.I. Alivov, C. Liu, A. Teke, M.A. Reshchikov, S. Doğan, V. Avrutin, S.J. Cho, H. Morko, A comprehensive review of ZnO materials and devices, J. Appl. Phys 98 (2005), 2005, pp. 1–103.
[46] V. Lacivita, A. Erba, Y. Noël, R. Orlando, P. D'Arco, R. Dovesi, Zinc oxide nanotubes: an ab initio investigation of their structural, vibrational, elastic, and dielectric properties, J. Chem. Phys. 138 (2013) (214706–214706-9).
[47] P.L. McEuen, J.Y. Park, Electron transport in single-walled carbon nanotubes, MRS Bull. 29 (2004) 272–275.
[48] J. Lim, B.G. Jeong, M. Park, J.K. Kim, J.M. Pietryga, Y.S. Park, V.I. Klimov, C. Lee, D.C. Lee, W.K. Bae, Influence of shell thickness on the performance of light-emitting devices based on CdSe/Zn 1- X Cd x S core/shell heterostructured quantum dots, Adv. Mater. 26 (2014) 8034–8040.
[49] Y. Yang, O. Chen, A. Angerhofer, Y.C. Cao, On doping CdS/ZnS core/shell nanocrystals with Mn, J. Am. Chem. Soc. 130 (2008) 15649–15661.
[50] C.W. Raubach, Y.V.B. De Santana, M.M. Ferrer, V.M. Longo, J.A. Varela, W. Avansi, P.G.C. Buzolin, J.R. Sambrano, E. Longo, Structural and optical approach of CdS@ZnS core-shell system, Chem. Phys. Lett. 536 (2012) 96–99.
[51] H.Y. Chen, S. Maiti, D.H. Son, Doping location-dependent energy transfer dynamics in Mn-doped CdS/ZnS nanocrystals, ACS Nano 6 (2012) 583–591.
[52] C.W. Raubach, L. Polastro, M.M. Ferrer, A. Perrin, C. Perrin, A.R. Albuquerque, P.G.C. Buzolin, J.R. Sambrano, Y.B.V. De Santana, J.A. Varela, E. Longo, Influence of solvent on the morphology and photocatalytic properties of ZnS decorated CeO2 nanoparticles, J. Appl. Phys. 115 (2014) (213514–213514-10).
[53] V.I. Klimov, Mechanisms for photogeneration and recombination of multiexcitons in semiconductor nanocrystals: implications for lasing and solar energy conversion, J. Phys. Chem. B 110 (2006) 16827–16845.
[54] B.O. Dabbousi, J. Rodriguez-Viejo, F.V. Mikulec, J.R. Heine, H. Mattoussi, R. Ober, K.F. Jensen, M.G. Bawendi, (CdSe)ZnS Core–shell quantum dots: synthesis and characterization of a size series of highly luminescent nanocrystallites, J. Phys. Chem. B 101 (1997) 9463–9475.
[55] N. Sai, E. Mele, Microscopic theory for nanotube piezoelectricity, Phys. Rev. B 68 (2003) 1–3.
[56] Z.C. Tu, X. Hu, Elasticity and piezoelectricity of zinc oxide crystals, single layers, and possible single-walled nanotubes, Phys. Rev. B: Condens. Matter 74 (2006) (035434–035434-6).